RSC Advances

PAPER

View Article Online
View Journal | View Issue

Cite this: RSC Adv., 2015, 5, 67718

Side chain structure affects the molecular packing and photovoltaic performance of oligothiophene-based solution-processable small molecules†

Shang-Che Lan,[a] Chiao-Kai Chang,[a] Yueh-Hsin Lu,[a] Shu-Wei Lin,[a] Alex K.-Y. Jen[b] and Kung-Hwa Wei*[a]

Received 29th June 2015
Accepted 27th July 2015

DOI: 10.1039/c5ra12540e

www.rsc.org/advances

In this study we synthesized a series of solution-processable small molecules comprising 2,2′-bithiophene (BTh), terthiophene (TTh), and thiobarbituric acid (TB) units as the central core, π-conjugated spacer, and acceptor end-capping moieties, respectively, but with alkyl side-chains of different lengths presented from their central BTh units (TBTThBTh-H, TBTThBTh-C4, TBTThBTh-C8, TBTThBTh-C12). We then investigated the structure–property relationships of these compounds in terms of their packing behaviors and bulk heterojunction (BHJ) photovoltaic properties. And we found that the packing of these molecules in neat films is critically dependent of their side-chain lengths, as evidenced by the variations in their lamellar structures determined with grazing-incidence wide-angle X-ray scattering (GIWAXS). The power conversion efficiencies (PCEs) of the photovoltaic BHJ devices comprising these small molecules and $PC_{61}BM$ exhibited zigzag-shaped variations with respect to the alkyl side-chain lengths, with the PCE of devices incorporating TBTThBTh-H and TBTThBTh-C8 being higher than those of devices incorporating TBTThBTh-C4 and TBTThBTh-C12. Using GIWAXS to probe the molecular packing in the BHJ active layers, we found that the alkyl chain lengths of the small molecules had a large impact on the formation of crystallites in the BHJ films; the molecules with more uniform and shorter alkyl side-chain lengths provide stronger intermolecular interactions, being more favorable for the crystallization of these molecules.

Introduction

Solution-processed organic photovoltaic (OPV) technology is a promising approach for alternative energy production because it offers the possibility of producing low-cost solar cells with rapid printing production techniques, even on flexible substrates.[1–3] Efficient solution-processed organic solar cells generally feature an active layer having a bulk heterojunction (BHJ) architecture, consisting of a suitable p-type material (*e.g.*, π-conjugated polymer or π-conjugated small molecule) and an n-type fullerene derivative (*e.g.*, $PC_{61}BM$). Polymer-based organic solar cells have attracted a great deal of attention over the past decade because they are readily fabricated through solution processing and because they display relatively high performance. Several significant approaches toward developing highly efficient solar cells have been established through advances in molecular design (*e.g.*, optimizing electronic properties[4–6] and crystallinity[7–9]), morphological control (*e.g.*, use of solvent additives),[10–14] interfacial engineering[15–17] and device engineering.[18–20]

p-type small molecules have also received much attention in photovoltaic applications because of their well-defined structures, ready purification, and lower batch-to-batch variation when compared with that of polymers. Typically, a photovoltaic device incorporating a polymer with higher molecular weight results in a better performance than that comprising a polymer with a lower molecular weight when the molecular weights of the polymers are smaller than a threshold molecular weight value as reported in the literatures,[21–23] because longer polymer chains can form a better percolated charge-transport network with fewer charge-trapping sites that arises from polymers' termini, within the BHJ active layer. Indeed, in some respects, we can consider small molecules as very low molecular weight polymers. Consequently, the charge transport in the BHJ active layer based on small molecules is highly dependent on the molecules' packing, crystallinity and their orientation.[24–27] Recently, some highly efficient BHJ devices have been prepared through solution processing using newly developed solution-processable molecules.[28–32] A PCE of 9.0% has been achieved

[a]Department of Materials Science and Engineering, National Chiao Tung University, 300 Hsinchu, Taiwan. E-mail: khwei@mail.nctu.edu.tw

[b]Department of Materials Science and Engineering, University of Washington, Seattle, WA, USA

† Electronic supplementary information (ESI) available: Experimental sections, and illustration of hypothetical lamellar configuration for molecules. See DOI: 10.1039/c5ra12540e

for a solar cell incorporating solution-processed small molecules,[33] virtually very close to the highest PCE (11.0%) published to date for a polymer solar cell.[34] These advanced molecules exhibit high crystallinity and appropriate phase separation with fullerene derivatives after optimizing the morphology of the BHJ layers.[35–37] Most highly efficient small molecules OPV, however, are still limited to molecules with some specific functional groups. It is thus critical to properly design the molecular structures that control a molecule's crystalline nature and its miscibility with fullerenes when developing efficient BHJ OPVs.[38,39]

Like conjugated polymers, small molecules require certain degrees of solubility in common solvents to afford solutions having desirable rheological properties; attaching alkyl side chains with various architectures, so-called side-chain engineering, is the most usual approach.[40,41] For polymeric systems, side-chain engineering influences the degree of molecular packing.[42–46] For solution-processed small molecules, the position[47–49] and also the length[50–52] of the side chain on the molecule can greatly impact its molecular crystallinity and the performance of its corresponding devices. In spite of these efforts, the studies of side-chain engineering for solution-processed small molecules OPV are still limited.

In a previous report, we described the synthesis of a series of solution-processed small molecules comprising an electron-donating moiety as the central core, terthiophene (TTh) units as π-conjugated spacers, and electron-accepting thiobarbituric acid (TB) units as end-capping moieties; we also investigated the impact of various core species on their molecular crystallinity and photovoltaic behavior.[53] Among those molecules, TBTThBTh-H, featuring a 2,2′-bithiophene (BTh) unit at its core, exhibited relatively poor solubility and resulted in devices with moderate efficiencies. In this present study, we instead investigated the effects of the side chains architectures in term of alkyl chain lengths on the structure–property relationships and photovoltaic properties of small molecules with the same main chain structure. Accordingly, we attached two additional alkyl chains with various lengths to the central BTh unit to increase and to vary the solubility of TBTThBTh molecules, thereby affording a series of molecules with different side chain architectures (Fig. 1) for this present study. The different side chain compositions of these molecules lead to variations in their molecular packing and photovoltaic properties.

Results and discussions

Solubility and thermal properties

All of the tested molecules are soluble in hot-toluene and $CHCl_3$, with the solubilities in chloroform following the order TBTThBTh-C12 > TBTThBTh-C8 > TBTThBTh-C4 > TBTThBTh-H (Table 1). As expected, longer alkyl chains led to significant increases in solubility. Nevertheless, all four of these molecules exhibited limited solubility in other common processing solvents (*e.g.*, chlorobenzene, *o*-dichlorobenzene). Fig. 2 displays differential scanning calorimetry (DSC) thermograms of these molecules; Table 1 lists their corresponding melting temperatures (T_m) and crystallization temperatures (T_c) that were obtained in the scan loop, which was initiated after the heat history of the samples had been erased. The values of both T_m and T_c followed the sequence TBTThBTh-H > TBTThBTh-C4 > TBTThBTh-C8 > TBTThBTh-C12. Upon increasing the alkyl chain length, the phase transition temperature decreased; meanwhile, the peak shape broadened and became featureless. We attribute these effects on thermal transitions to the longer alkyl chains decreasing the molecular cohesive energy and increasing the degree of disorder in the solid state. We also probed the liquid-crystal properties of these molecules with polarizing optical microscopy and found no such properties.[54]

Optical and electrochemical properties

Fig. 3 presents normalized UV-vis absorption spectra of the TBTThBTh molecules in $CHCl_3$ solutions and in the film state; Table 2 summarizes the optical properties. The absorption spectra of dilute solutions of the TBTThBTh molecules feature similar absorption peaks near 445 and 565 nm. The features in these spectra underwent broadening and red-shifting upon

Table 1 Phase transition temperatures and solubilities of TBTThBTh molecules

Molecule	Phase transition temperature		Solubility in $CHCl_3$ (mg mL^{-1})
	T_m [°C]	T_c [°C]	
TBTThBTh-H	227	174	6.3
TBTThBTh-C4	182, 203, 208	157, 169	10.2
TBTThBTh-C8	181	149, 163	12.5
TBTThBTh-C12	119, 163	139	14.6

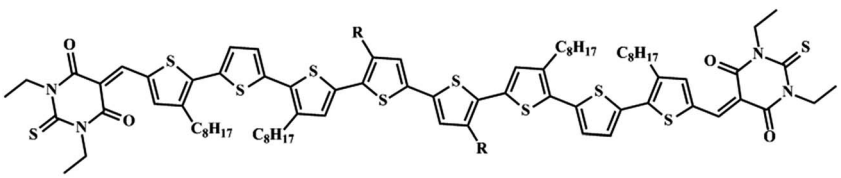

TBTThBTh-H : R = H **TBTThBTh-C8** :R = C_8H_{17}

TBTThBTh-C4 : R = C_4H_9 **TBTThBTh-C12** :R = $C_{12}H_{25}$

Fig. 1 Structures of the tested TBTThBTh molecules.

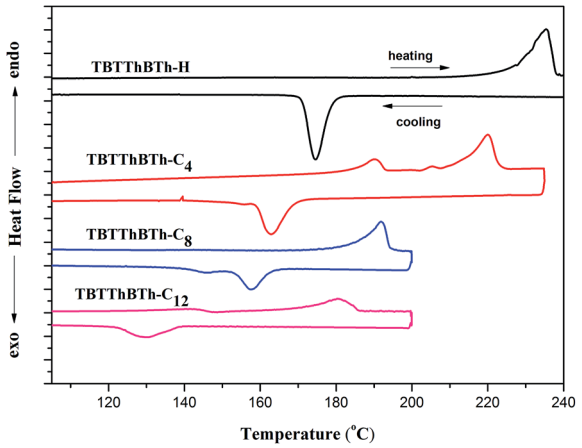

Fig. 2 DSC thermograms of TBTThBTh molecules. Upper line: heating scan; lower line: cooling scan (heating rate: 5 °C min^{-1}).

proceeding from dilute solutions to thin films, presumably because of strong intermolecular interactions in the solid state. We observed, however, different degrees of spectral change among the tested molecules, with molecules featuring longer alkyl chains exhibiting smaller changes between their spectra recorded in solution and from a thin film. As a result, TBTThBTh-C12 displayed the narrowest spectrum window and a slightly wide bandgap, possibly because its longer alkyl chains prevented intermolecular π–π interactions or disrupted its backbone coplanarity in the solid state. We used cyclic voltammetry (CV) to determine the energy levels of the highest occupied molecular orbitals (HOMOs) of these molecules; Table 2 lists the pertinent numerical data. The variations in HOMO energy levels among the four molecules were minor; in other words, the length of the alkyl chains had negligible impact on the energy levels in this study.

Molecular packing

To investigate the influence of our side-chain modifications on molecular packing, we performed grazing-incidence wide-angle X-ray scattering (GIWAXS) analyses on neat films of our molecules. Fig. 4 displays the GIWAXS 2D-patterns of molecules, and a 1D-patterns obtained by azimuthally integrating form 90–180° of 2D images. In the low-q range (2–5 nm^{-1}), the films of TBTThBTh-C4 and TBTThBTh-C8 each featured two diffraction peaks, whereas those of TBTThBTh-H and TBTThBTh-C12 each exhibited a broad peak that consisted of two peaks, as evidenced by comparing the 1D-patterns recorded out-of-plane and in-plane (Fig. S3†). Meanwhile, there are also two broad reflection singles existed in the high-q range of 12–20 nm^{-1} for our molecules. Table 3 lists the corresponding d-spacings of these peaks for each molecule. Although the single crystal structures of our molecules are unknown, lamellar stacking, a typical stacking configuration for crystalline polymers, is the most common crystal architecture for β-alkyl oligothiophenes.[55–57] If our molecules underwent lamellar stacking, they possibly adopted two kind of lamellar-type stacking configurations within the films because of the d-spacings of Peaks I and II for each molecule that cannot be classified into a set of plan, and hence these two peaks (Peaks I and II) are the diffraction peaks arose from different (100) plane.

Furthermore, the variations of d-spacings of these four small molecules give us some interesting features about the alkyl stacking. TBTThBTh-C4 and TBTThBTh-C8 have the shorter $d_{(100)}$-spacing on Peak I and II than the other two small molecules, which implying that TBTThBTh-C4 and TBTThBTh-C8 could form relatively highly interdigitated lamellar structures particularly for TBTThBTh-C8, which preferred to adopt such a configuration, as evidenced by comparing the intensities of Peaks I and II. Although we might predict that the spacing in the film of TBTThBTh-C12 would be larger among four molecules, because the former possessed the longest alkyl chains, the film of TBTThBTh-H, which featured the common octane units as its longest side chains, had the same spacing as that of TBTThBTh-C12, rather than that of TBTThBTh-C8. The possible reason is that TBTThBTh-H has less substituted positions of alkyl chain, inducing weaker hydrophobic interactions. Because assembly through lamellar stacking occurs through hydrophobic alkyl–alkyl interactions, the chain length and the concentration of the substituents should both affect the structure. When we increased the length of the central alkyl chains, upon proceeding from TBTThBTh-H to TBTThBTh-C8, we expected to that increasing concentration of the substituents and equalizing side-chain length both enforce molecules on forming more closed lamellar-stacking; hence, TBTThBTh-H formed a

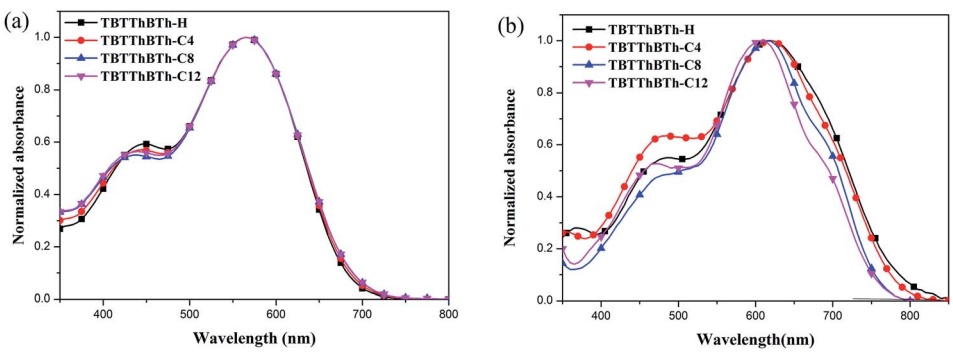

Fig. 3 UV-vis absorption spectra of TBTThBTh molecules in the form of (a) solutions in $CHCl_3$ and (b) as-cast films.

Table 2 Optical and electrochemical properties of TB3tBT molecules

	Optical properties					
	Solution[a]	Film[b]			Energy levels[d]	
Molecule	λ_{max} [nm]	λ_{max} [nm]	λ_{onset} [nm]	E_g^{optc} [eV]	HOMO [eV]	LUMO [eV]
TB3tBT-H	447, 565	483, 620	781	1.59	−5.12	−3.59
TB3tBT-C4	445, 565	476, 620	779	1.59	−5.15	−3.63
TB3tBT-C8	455, 565	474, 616	768	1.61	−5.20	−3.54
TB3tBT-C12	445, 565	468, 606	765	1.62	−5.20	−3.62

[a] Dilute solution in $CHCl_3$. [b] Spin-coated from $CHCl_3$ onto ITO/PEDOT substrates. [c] Optical band gaps calculated from $E_g = 1240/\lambda_{onset}$ eV. [d] Energy levels determined from onsets of the CV curves: energy levels $= -(4.8 + E_{onset})$ eV.

structure having the lowest degree of interdigitation. Additionally, we proposed hypothetical illustrations of lamellar stacking base on concept of hydrophobic alkyl–alkyl interactions for our molecules, and provided in the ESI.†

Photovoltaic properties

We use a conventional device structure to evaluate the photovoltaic properties of these molecules. We optimized the device performance for each individual molecule in terms of the film thickness by varying the solution concentration, the molecule-to-fullerene ratio, and the annealing temperature; Table 4 lists the averaged photovoltaic parameters obtained from 20 cells. Thermal annealing was a critical step for improving the device performance; devices in the pristine condition displayed unsatisfactory efficiencies (PCE: <1%) because of the amorphous nature of the molecules in the as-cast blend films. The influence of the annealing conditions was consistent with the phase transition temperatures of the individual molecules. Among devices incorporating the molecule/$PC_{61}BM$ blends, the

Table 3 *d*-Spacings of TBTThBTh-type small molecules

	Alkyl chain stacking		π stacking	
	d-Spacing (Å) of (100)		*d*-Spacing (Å) of (010)	
Molecule	Peak I	Peak II	Peak III	Peak IV
TBTThBTh-H	26.2	20.9	4.7	3.7
TBTThBTh-C4	23.3	18.0	4.6	3.7
TBTThBTh-C8	25.1	18.0	4.6	3.8
TBTThBTh-C12	26.2	20.9	4.5	3.7

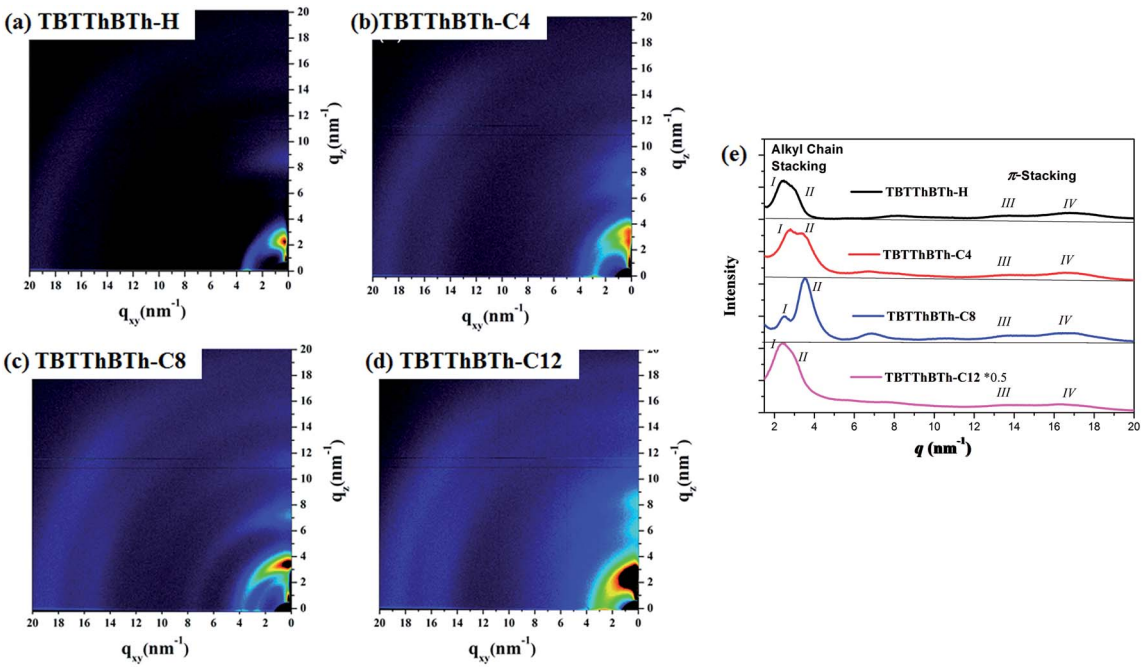

Fig. 4 (a–d) 2D GIWAXS images of annealed neat films of (a) TBTThBTh-H, (b) TBTThBTh-C4, (c) TBTThBTh-C8, and (d) TBTThBTh-C12. (e) One-dimensional powder diffraction traces generated by azimuthally integrating GIWAXS images.

devices featuring TBTThBTh-H exhibited the best performance and a moderate PCE of 3.7%, with an open-circuit voltage (V_{OC}) of 0.89 V, a short-circuit current density (J_{SC}) of 8.3 mA cm^{-2}, and a fill factor (FF) of 50%. When $PC_{71}BM$ replaced $PC_{61}BM$ in the blend films with TBTThBTh-H, the PCE of the optimal device improved to 4.3% as a result of increasing the value of J_{SC} (from 8.3 to 9.4 mA cm^{-2}).

Fig. 5 displays the relative differences in performance, compared with that of TBTThBTh-H, for the devices incorporating the small molecules featuring longer central side chains. Although the overall efficiencies decreased, the variations in the photovoltaic parameters among the four small molecules zigzagged upon increasing the length of the central side chains. The device performances of TBTThBTh-C4 and TBTThBTh-C12 exhibited obvious declines, whereas the devices incorporating TBTThBTh-C8 functioned comparatively better. The correlation between the photovoltaic parameters and the length of the molecular side chain remains unclear.

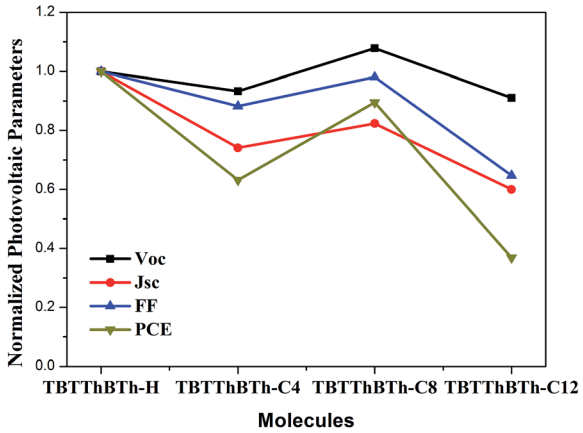

Fig. 5 Relative differences in photovoltaic parameters of solar cells incorporating the four small molecules, compared with those obtained using TBTThBTh-H.

TEM images of small molecule/$PC_{61}BM$ blends

We used transmission electron microscopy (TEM) to examine the influence of the side chain composition of the molecules on the BHJ morphologies (Fig. 6). All of the annealed films featured rod-like crystalline domains distributed in the matrix, with fibrils penetrating into the fullerene-rich region to increase the interfacial area between the organic molecules and the fullerenes. We would expect this type of morphology to assist not only exciton separation but also charge transport; hence, the annealing process ensured reasonable PCEs for all of the devices. We observed another interesting feature in that the phase separation of the small molecules and fullerenes became more complicated and clear upon increasing the alkyl chain length on the central unit. The films of TBTThBTh-H showed most ideal phase separation, leading best efficiency. Then, the films of TBTThBTh-C8 and TBTThBTh-C12 contained relatively large domains of molecular aggregation (white regions); as a result, the values of J_{SC} and FF of their devices decreased because of the lower interfacial area and consequently lower degrees of charge separation. This phenomenon is consistent with the results of previous studies[58–60] increasing the alkyl chain length of a conjugated material tends to decrease its miscibility with $PC_{61}BM$.

Crystallization in small molecule/$PC_{61}BM$ blends

To further investigate the morphologies of the four active layers, we employed GIWAXS to inspect crystallization behaviors of our molecules in the blend films. Fig. 7 displays the 2D patterns of the blend films together with the profiles of their out-of-plane (q_z) integrations. All samples exhibited strong diffraction in the out-of-plane region, implying that the small molecules favored an edge-on orientation in the active layer. However, the case of TBTThBTh-H showed that the crystallites adopt comparatively random orientation, as evident by a ring-typed diffraction pattern appeared in images, and such random orientation is slightly undesirable for charge transport.[10] Then we focus on the discussion on the effect of the size and stacking order of the molecular crystallites in the BHJ films on the photovoltaic performances of the devices incorporating these films. We found that the X-ray diffraction curves (Fig. 7(e)) of all molecules except TBTThBTh-C12 present highly ordered peaks, implying TBTThBTh-C12 molecule possessed more amorphous characteristics than that of other molecules. Furthermore, we used the primary X-ray diffraction peaks with Scherrer equation for calculating the crystallite correlation lengths (CCL) for our molecules, and the corresponding correlation lengths were given in Table 5.[61] It is interesting that the trend in the values of CCL varies substantially, indicating the different alkyl side-chain lengths induce the different CCL values. The CCL trend—CCL(TBTThBTh-H) > CCL(TBTThBTh-C8) > CCL(TBTThBTh-C4) > CCL(TBTThBTh-12)—was the same as that of the trend of J_{SC} and FF. We thus suspect that more uniform alkyl side-chain lengths, in this case there are octyl chains on the thiophene as well, and shorter alkyl side-chain lengths, which provide

Table 4 Photovoltaic properties of OPVs incorporating TBTThBTh-type small molecule/PCBM blends

Small molecule	Fullerene	Annealing (temp., time)	V_{OC} (V)	J_{SC} (mA cm^{-2})	FF (%)	PCE (%)
TBTThBTh-H	$PC_{61}BM$	150 °C, 15 min	0.89	8.3	50	3.7
	$PC_{71}BM$		0.89	9.4	51	4.3
TBTThBTh-C4	$PC_{61}BM$	120 °C, 10 min	0.83	6.3	45	2.4
TBTThBTh-C8	$PC_{61}BM$	120 °C, 10 min	0.95	7.0	48	3.2
TBTThBTh-C12	$PC_{61}BM$	100 °C, 10 min	0.81	5.1	33	1.4

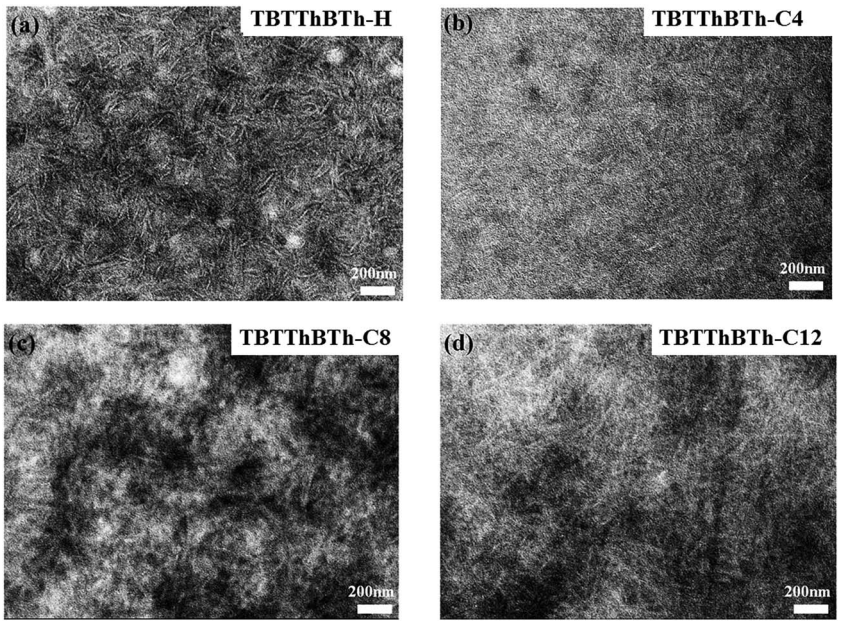

Fig. 6 TEM images of annealed active layers of (a) TBTThBTh-H/$PC_{61}BM$, (b) TBTThBTh-C4/$PC_{61}BM$, (c) TBTThBTh-C8/$PC_{61}BM$, and (d) TBTThBTh-C12/$PC_{61}BM$.

stronger intermolecular interactions, are more favorable for the crystallization of these molecules.

On the hand, we calculated the corresponding *d*-spacing for each diffraction pattern in the *q*-region of 2–12 nm^{-1}. The corresponding *d*-spacings of each peak were labeled in Fig. 7(e). These *d*-spacings suggest that TBTThBTh-H and TBTThBTh-C8 mainly adopted lamellar structures of Peak II in their active layers, while TBTThBTh-C4 and TBTThBTh-C12 could be characterized as having the structures of Peak I. Furthermore, it is interesting that the variations in *d*-spacings are very similar to those for the values of V_{OC}. From the Shockley equation for the current–voltage (*J*–*V*) characteristics of a solar cell under

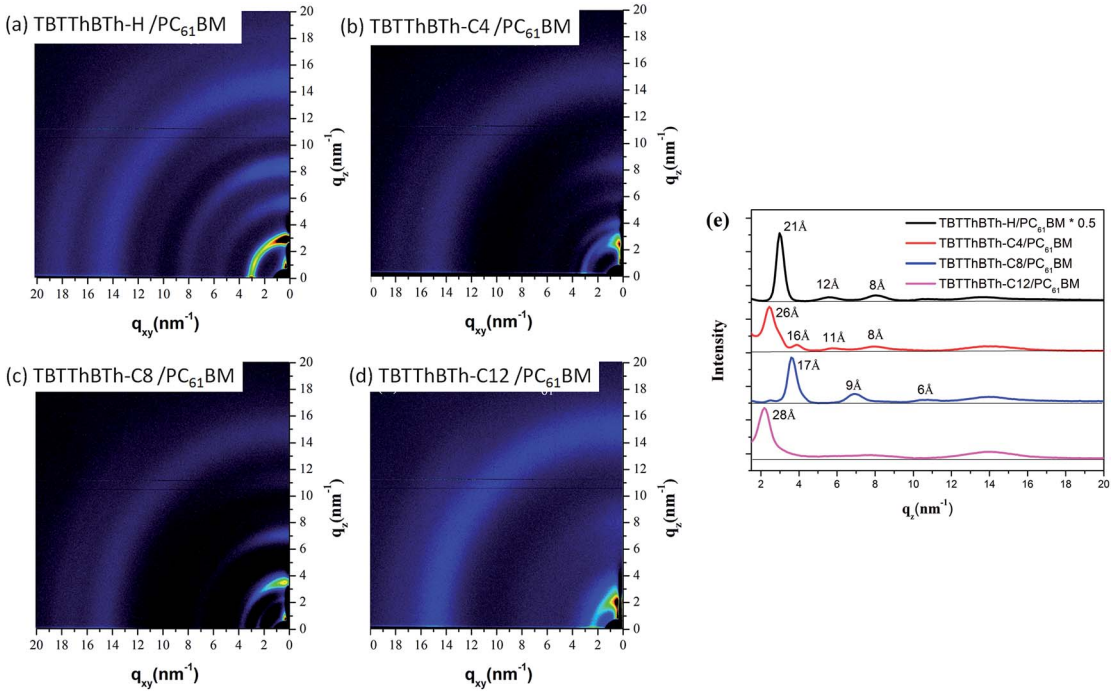

Fig. 7 (a–d) 2D GIWAXS images of annealed active layers of (a) TBTThBTh-H/$PC_{61}BM$, (b) TBTThBTh-C4/$PC_{61}BM$, (c) TBTThBTh-C8/$PC_{61}BM$, and (d) TBTThBTh-C12/$PC_{61}BM$. (e) Out-of-plane scans of GIWAXS images.

Table 5 FWHM and crystallites correlation lengths of primary peaks from 1D out-of-plane GIWAXS profiles

Molecules	FWHM (nm^{-1})	CCL (nm)
TBTThBTh-H	0.47	12.03
TBTThBTh-C4	0.66	8.44
TBTThBTh-C8	0.54	10.56
TBTThBTh-C12	0.80	7.01

illumination, V_{OC}[62–65] can be written as the voltage V measured at the condition at zero current ($J = 0$),

$$eV_{OC} = nk_BT \ln(J_{SC}/J_0 + 1) \quad (1)$$

where J_{SC} denotes the short circuit current, J_0 is the reverse saturation current, n is the ideality factor, and k_B is Boltzmann's constant. Then the J_0 can be further expressed as:

$$J_0 = J_{SO} \exp(-\Delta E/nk_BT) \quad (2)$$

By combining equations of (1) and (2), the V_{OC} can be rewritten as:

$$eV_{OC} \sim \Delta E - nk_BT \ln(J_{SO}/J_{SC}) \quad (3)$$

where ΔE is the energy offset between LUMO level of n-typed materials and HOMO level of p-typed materials, and the J_{SO} is related to the reorganization energy and intermolecular overlap at the D/A interface that determine the carrier generation/recombination rate, independent of ΔE. Eqn (3) implies that V_{OC} is determined by ΔE and the interaction of p–n junctions. Based on the analysis the values of molecular d-spacing, our molecules have different packing structures within the BHJ layers, and thus this different packing might cause different interfacial energy of D/A interfaces, giving different values of V_{OC}.[61] And we found in this study that a molecule with higher degree of interdigitation, referring more ideal lamellar, have higher value of V_{OC}.

Conclusions

After synthesizing a series of TBTThBTh-based solution-processable small molecules having side chains of different lengths on their central BT units, we investigated their crystallization characteristics as well as their BHJ photovoltaic properties when blended with fullerenes. Upon increasing the length of the central side chain, the small molecules became increasingly soluble, while their phase transition temperatures (T_m, T_c) decreased accordingly. Nevertheless, films of these small molecules displayed two diffraction peaks of the (100) plane in their GIWAXS patterns, indicating polymorphism. Interestingly, the relative intensity of these two peaks changed when we modified the length of the central side chain, suggesting that it also affected the preferred stacking of the small molecules.

The photovoltaic properties were affected significantly by the side-chain modifications. TEM analysis revealed that the small molecules featuring longer alkyl chains were less miscible with $PC_{61}BM$, and the case of TBTThBTh-H/$PC_{61}BM$ showed most ideal phase separation and highest efficiency. As for the others, the values of J_{SC} and FF decreased because of the unfavorable morphology for charge separation. Through GIWAXS analyses of the molecular packing in the active layers, we found that the alkyl chain architectures of the small molecules had impact on the formation of crystallites in the BHJ films as well as the photovoltaic performances of devices incorporating them.

Acknowledgements

The authors thank Hsiu-Cheng Chen for assistance with the TEM analysis and the National Science Council, Taiwan, for financial support (NSC 101-2923-E-009-003-MY3).

References

1 G. Li, R. Zhu and Y. Yang, *Nat. Photonics*, 2012, **6**, 153–161.
2 Y.-W. Su, S.-C. Lan and K.-H. Wei, *Mater. Today*, 2012, **15**, 554–562.
3 N. Espinosa, M. Hösel, M. Jørgensen and F. C. Krebs, *Energy Environ. Sci.*, 2014, **7**, 855–866.
4 H. Zhou, L. Yang and W. You, *Macromolecules*, 2012, **45**, 607–632.
5 K. C. Li, Y. C. Hsu, J. T. S. Lin, C. C. Yang, K. H. Wei and H. C. Lin, *J. Polym. Sci., Part A: Polym. Chem.*, 2009, **47**, 2073–2092.
6 J.-M. Jiang, H.-C. Chen, H.-K. Lin, C.-M. Yu, S.-C. Lan, C.-M. Liu and K.-H. Wei, *Polym. Chem.*, 2013, **4**, 5321–5328.
7 Y. Wu, Z. Li, W. Ma, Y. Huang, L. Huo, X. Guo, M. Zhang, H. Ade and J. Hou, *Adv. Mater.*, 2013, **25**, 3449–3455.
8 W. Lee, G.-H. Kim, S. Ko, S. Yum, S. Hwang, S. Cho, Y. Shin, J. Y. Kim and H. Y. Woo, *Macromolecules*, 2014, **47**, 1604–1612.
9 S.-C. Lan, P.-A. Yang, M.-J. Zhu, C.-M. Yu, J.-M. Jiang and K.-H. Wei, *Polym. Chem.*, 2013, **4**, 1132–1140.
10 J. Rivnay, S. C. B. Mannsfeld, C. E. Miller, A. Salleo and M. F. Toney, *Chem. Rev.*, 2012, **112**, 5488–5519.
11 Y. Huang, E. J. Kramer, A. J. Heeger and G. C. Bazan, *Chem. Rev.*, 2014, **114**, 7006–7043.
12 C.-M. Liu, Y.-W. Su, J.-M. Jiang, H.-C. Chen, S.-W. Lin, C.-J. Su, U.-S. Jeng and K.-H. Wei, *J. Mater. Chem. A*, 2014, **2**, 20760–20769.
13 C.-M. Liu, M.-S. Su, J.-M. Jiang, Y.-W. Su, C.-J. Su, C.-Y. Chen, C.-S. Tsao and K.-H. Wei, *ACS Appl. Mater. Interfaces*, 2013, **5**, 5413–5422.
14 H.-S. Wang, L.-H. Lin, S.-Y. Chen, Y.-L. Wang and K.-H. Wei, *Nanotechnology*, 2009, **20**, 075201–075205.
15 S. Liu, K. Zhang, J. Lu, J. Zhang, H.-L. Yip, F. Huang and Y. Cao, *J. Am. Chem. Soc.*, 2013, **135**, 15326–15329.
16 H.-L. Yip and A. K.-Y. Jen, *Energy Environ. Sci.*, 2012, **5**, 5994–6011.
17 C. E. Small, S. Chen, J. Subbiah, C. M. Amb, S.-W. Tsang, T.-H. Lai, J. R. Reynolds and F. So, *Nat. Photonics*, 2011, **6**, 115–120.

18 J. You, L. Dou, K. Yoshimura, T. Kato, K. Ohya, T. Moriarty, K. Emery, C.-C. Chen, J. Gao, G. Li and Y. Yang, *Nat. Commun.*, 2013, **4**, 1446–1449.
19 W. Li, A. Furlan, K. H. Hendriks, M. M. Wienk and R. A. J. Janssen, *J. Am. Chem. Soc.*, 2013, **135**, 5529–5532.
20 C.-C. Chen, W.-H. Chang, K. Yoshimura, K. Ohya, J. You, J. Gao, Z. Hong and Y. Yang, *Adv. Mater.*, 2014, **26**, 5670–5677.
21 J. J. Intemann, K. Yao, H. L. Yip, Y. X. Xu, Y. X. Li, P. W. Liang, F. Z. Ding, X. Li and A. K. Y. Jen, *Chem. Mater.*, 2013, **25**, 3188–3195.
22 J. A. Bartelt, J. D. Douglas, W. R. Mateker, A. El Labban, C. J. Tassone, M. F. Toney, J. M. J. Fréchet, P. M. Beaujuge and M. D. McGehee, *Adv. Energy Mater.*, 2014, **4**, 1301733–1301744.
23 W. Li, L. Yang, J. R. Tumbleston, L. Yan, H. Ade and W. You, *Adv. Mater.*, 2014, **26**, 4456–4462.
24 B. R. Kaafarani, *Chem. Mater.*, 2011, **23**, 378–396.
25 N. D. Eisenmenger, G. M. Su, G. C. Welch, C. J. Takacs, G. C. Bazan, E. J. Kramer and M. L. Chabinyc, *Chem. Mater.*, 2013, **25**, 1688–1698.
26 J. Liu, B. Walker, A. Tamayo, Y. Zhang and T.-Q. Nguyen, *Adv. Funct. Mater.*, 2013, **23**, 47–56.
27 C. J. Takacs, S. D. Collins, J. A. Love, A. A. Mikhailovsky, D. Wynands, G. C. Bazan, T.-Q. Nguyen and A. J. Heeger, *ACS Nano*, 2014, **8**, 8141–8151.
28 T. S. van der Poll, J. A. Love, T.-Q. Nguyen and G. C. Bazan, *Adv. Mater.*, 2012, **24**, 3646–3649.
29 Y. Liu, X. Wan, F. Wang, J. Zhou, G. Long, J. Tian, J. You, Y. Yang and Y. Chen, *Adv. Energy Mater.*, 2011, **1**, 771–775.
30 Y. Liu, Y. M. Yang, C. C. Chen, Q. Chen, L. Dou, Z. Hong, G. Li and Y. Yang, *Adv. Mater.*, 2013, **25**, 4657–4662.
31 D. Patra, C.-C. Chiang, W.-A. Chen, K.-H. Wei, M.-C. Wu and C.-W. Chu, *J. Mater. Chem. A*, 2013, **1**, 7767–7774.
32 H. Qin, L. Li, F. Guo, S. Su, J. Peng, Y. Cao and X. Peng, *Energy Environ. Sci.*, 2014, **7**, 1397–1401.
33 B. Kan, Q. Zhang, M. Li, X. Wan, W. Ni, G. Long, Y. Wang, X. Yang, H. Feng and Y. Chen, *J. Am. Chem. Soc.*, 2014, **136**, 15529–15532.
34 J.-D. Chen, C. Cui, Y.-Q. Li, L. Zhou, Q.-D. Ou, C. Li, Y. Li and J.-X. Tang, *Adv. Mater.*, 2015, **27**, 1035–1041.
35 L. A. Perez, J. T. Rogers, M. a. Brady, Y. Sun, G. C. Welch, K. Schmidt, M. F. Toney, H. Jinnai, A. J. Heeger, M. L. Chabinyc, G. C. Bazan and E. J. Kramer, *Chem. Mater.*, 2014, **26**, 6531–6541.
36 W. Ni, M. Li, X. Wan, H. Feng, B. Kan, Y. Zuo and Y. Chen, *RSC Adv.*, 2014, **4**, 31977–31980.
37 J. Zhou, X. Wan, Y. Liu, Y. Zuo, Z. Li, G. He, G. Long, W. Ni, C. Li, X. Su and Y. Chen, *J. Am. Chem. Soc.*, 2012, **134**, 16345–16351.
38 A. Viterisi, F. Gispert-Guirado, J. W. Ryan and E. Palomares, *J. Mater. Chem.*, 2012, **22**, 15175–15182.
39 K. R. Graham, R. Stalder, P. M. Wieruszewski, D. G. Patel, D. H. Salazar and J. R. Reynolds, *ACS Appl. Mater. Interfaces*, 2012, **5**, 63–71.
40 M.-C. Yuan, M.-Y. Chiu, S.-P. Liu, C.-M. Chen and K.-H. Wei, *Macromolecules*, 2010, **43**, 6936–6938.
41 G.-Y. Chen, Y.-H. Cheng, Y.-J. Chou, M.-S. Su, C.-M. Chen and K.-H. Wei, *Chem. Commun.*, 2011, **47**, 5064–5066.
42 L. Fang, Y. Zhou, Y.-X. Yao, Y. Diao, W.-Y. Lee, A. L. Appleton, R. Allen, J. Reinspach, S. C. B. Mannsfeld and Z. Bao, *Chem. Mater.*, 2013, **25**, 4874–4880.
43 I. Osaka, M. Saito, T. Koganezawa and K. Takimiya, *Adv. Mater.*, 2014, **26**, 331–338.
44 J. Mei and Z. Bao, *Chem. Mater.*, 2014, **26**, 604–615.
45 T. Lei, J.-Y. Wang and J. Pei, *Chem. Mater.*, 2014, **26**, 594–603.
46 S.-C. Lan, C.-K. Chang, Y.-C. Wang and K.-H. Wei, *ChemPhysChem*, 2015, **6**, 1268–1274.
47 V. S. Gevaerts, E. M. Herzig, M. Kirkus, K. H. Hendriks, M. M. Wienk, J. Perlich, P. Müller-Buschbaum and R. A. J. Janssen, *Chem. Mater.*, 2014, **26**, 916–926.
48 Y. S. Choi, T. J. Shin and W. H. Jo, *ACS Appl. Mater. Interfaces*, 2014, **6**, 20035–20042.
49 M. Jung, Y. Yoon, J. H. Park, W. Cha, A. Kim, J. Kang, S. Gautam, D. Seo, J. H. Cho, H. Kim, J. Y. Choi, K. H. Chae, K. Kwak, H. J. Son, M. J. Ko, H. Kim, D. K. Lee, J. Y. Kim, D. H. Choi and B. Kim, *ACS Nano*, 2014, **8**, 5988–6003.
50 D. Ye, X. Li, L. Yan, W. Zhang, Z. Hu, Y. Liang, J. Fang, W.-Y. Wong and X. Wang, *J. Mater. Chem. A*, 2013, **1**, 7622–7629.
51 Z. Li, J. Bian, Y. Wang, F. Jiang, G. Liang and P. He, *Sol. Energy Mater. Sol. Cells*, 2014, **130**, 336–346.
52 J. Min, Y. N. Luponosov, A. Gerl, M. S. Polinskaya, S. M. Peregudova, P. V Dmitryakov, A. V Bakirov, M. A. Shcherbina, S. N. Chvalun, S. Grigorian, N. Kaush-Busies, S. A. Ponomarenko, T. Ameri and C. J. Brabec, *Adv. Energy Mater.*, 2014, **4**, 1301234, DOI: 10.1002/aenm.201301234.
53 S.-C. Lan, P. Raghunath, Y.-H. Lu, Y.-C. Wang, S.-W. Lin, C.-M. Liu, J.-M. Jiang, M.-C. Lin and K.-H. Wei, *ACS Appl. Mater. Interfaces*, 2014, **6**, 9298–9306.
54 N. Hu, R. Shao, C. Zhu, Y. Shen, C. Park, E. Korblova, C. Guerra, J. A. Rego, A. Hexemer, N. A. Clark and D. M. Walba, *Chem. Sci.*, 2014, **5**, 1869–1874.
55 R. Azumi, G. Götz, T. Debaerdemaeker and P. Bäuerle, *Chem.–Eur. J.*, 2000, **6**, 735–744.
56 L. Zhang, N. S. Colella, F. Liu, S. Trahan, J. K. Baral, H. H. Winter, S. C. B. Mannsfeld and A. L. Briseno, *J. Am. Chem. Soc.*, 2013, **135**, 844–854.
57 L. Zhang, N. S. Colella, B. P. Cherniawski, S. C. B. Mannsfeld and A. L. Briseno, *ACS Appl. Mater. Interfaces*, 2014, **6**, 5327–5343.
58 Y. Deng, Y. Chen, J. Liu, L. Liu, H. Tian, Z. Xie, Y. Geng and F. Wang, *ACS Appl. Mater. Interfaces*, 2013, **5**, 5741–5747.
59 C.-C. Ho, S.-Y. Chang, T.-C. Huang, C.-A. Chen, H.-C. Liao, Y.-F. Chen and W.-F. Su, *Polym. Chem.*, 2013, **4**, 5351–5360.
60 H. Bronstein, D. S. Leem, R. Hamilton, P. Woebkenberg, S. King, W. Zhang, R. S. Ashraf, M. Heeney, T. D. Anthopoulos, J. de Mello and I. McCulloch, *Macromolecules*, 2011, **44**, 6649–6652.
61 C.-K. Mai, R. A. Schlitz, G. M. Su, D. Spitzer, X. Wang, S. L. Fronk, D. G. Cahill, M. L. Chabinyc and G. C. Bazan, *J. Am. Chem. Soc.*, 2014, **136**, 13478–13481.

62 M. Dolores Perez, C. Borek, S. R. Forrest and M. E. Thompson, *J. Am. Chem. Soc.*, 2009, **131**, 9281–9286.
63 S. Yamamoto, A. Orimo, H. Ohkita, H. Benten and S. Ito, *Adv. Energy Mater.*, 2012, **2**, 229–237.
64 C. W. Schlenker and M. E. Thompson, *Chem. Commun.*, 2011, **47**, 3702–3716.
65 U. Hörmann, C. Lorch, A. Hinderhofer, A. Gerlach, M. Gruber, J. Kraus, B. Sykora, S. Grob, T. Linderl, A. Wilke, A. Opitz, R. Hansson, A. S. Anselmo, Y. Ozawa, Y. Nakayama, H. Ishii, N. Koch, E. Moons, F. Schreiber and W. Brütting, *J. Phys. Chem. C*, 2014, **118**, 26462–26470.